PCCP

Shape Selective Properties of the Al-Fumarate Metal-Organic Framework in the Adsorption and Separation of n-Alkanes, iso-Alkanes, cyclo-Alkanes and Aromatic Hydrocarbons

Journal:	*Physical Chemistry Chemical Physics*
Manuscript ID	CP-ART-10-2015-006342.R1
Article Type:	Paper
Date Submitted by the Author:	18-Dec-2015
Complete List of Authors:	Bozbiyik, Belgin; Vrije Universiteit Brussel, Chemical Engineering Lannoeye, Jeroen; K.U.Leuven, Centre for Surface Chemistry and Catalysis De Vos, Dirk; K.U.Leuven, Centre for Surface Chemistry and Catalysis Baron, Gino; Vrije Universiteit Brussel, Chemical Engineering Denayer, Joeri F M; Vrije Universiteit Brussel, Chemical Engineering

Shape Selective Properties of the Al-Fumarate Metal-Organic Framework in the Adsorption and Separation of *n*-Alkanes, iso-Alkanes, cyclo-Alkanes and Aromatic Hydrocarbons

Belgin Bozbiyik[a], Jeroen Lannoeye[b], Dirk E. De Vos[b], Gino V. Baron[a] and Joeri F.M. Denayer[a,*]

[a] Department of Chemical Engineering, Vrije Universiteit Brussel, Pleinlaan 2, 1050 Brussel, Belgium.

[b] Centre for Surface Chemistry and Catalysis, Katholieke Universiteit Leuven, Kasteelpark Arenberg 23, 3001 Leuven, Belgium.

* Corresponding author email:Joeri.denayer@vub.ac.be

Abstract

The primary goal of this work is to study the adsorption of a wide range of hydrocarbon adsorbates in the Al-Fumarate Metal-Organic Framework in order to identify and explore trends in adsorption behaviour that can be related to the sorbate's molecular properties and as well as the properties of this MOF. The pulse chromatographic technique was used to study the adsorption properties of C5-C8 linear, branched, cyclic and aromatic hydrocarbons in vapour phase at low coverage and at high temperatures (150°C-250°C). Chromatograms of alkanes having the same number of carbon atoms (C_5-C_8) clearly show that the linear alkane is retained the longest over its branched and cyclic isomers. Moreover, xylene isomers are also clearly separated by Al-Fumarate, with retention times increasing in the order: ortho-xylene < meta-xylene < para-xylene. Differences in adsorption enthalpy of more than 10 kJ/mol between linear alkanes and their di/tri-branched or cyclo-alkane isomers were observed, clearly showing that steric effects imposed by the pore structure of the adsorbent cause the difference in adsorption between linear alkanes and their isomers. In conclusion, Al-Fumarate behaves as a shape selective material with respect to structural isomers of linear alkanes, with properties resembling those of medium pore size zeolites.

Key words: adsorption, MOF, Al-Fumarate, inverse pulse chromatography, shape selectivity, alkanes, iso-alkanes, aromatics, xylene isomers

Introduction

Microporous materials like zeolites are generally used in the petroleum industries to carry out the adsorptive separation or catalytic conversion of hydrocarbon isomers, based on the ability to selectively adsorb guest molecules in the micropores[1,2]. The size of the pores and the shape of the molecules guide this behaviour, known as molecular shape selectivity[3]. During such shape selective molecular separation, certain molecules of the feed mixture are only weakly adsorbed or even prevented from entering the pores while other components match well with the pores in the zeolite. A well-know application of this shape selective behaviour is the separation of linear and branched alkane isomers to improve the octane number of gasoline[4].

In most cases, the less bulky isomers are adsorbed preferentially in terms of adsorption equilibrium and kinetics[5–7]. Branched alkanes are less favourably adsorbed than their linear isomers because of steric hindrance effects, restraining branched alkanes to adopt an ideal adsorptive configuration[8,9].

Such shape selective properties have also been reported for Metal-Organic Frameworks (MOFs), also called Porous Coordination Polymers (PCP). MOFs are inorganic-organic hybrid materials. They have a porous structure built up from single metal ions or polynuclear metal clusters linked by organic ligands. The presence of strong coordination bonds between the metal centers and the organic linkers provides a geometrically and crystallographically well-defined framework structure with a high specific area [10]. Moreover, thanks to the capacity of tailor-made synthesis of MOFs by changing the metal centers or the organic ligands, morphological and chemical properties like pore size and shape, composition of the framework and presence of functional groups within the pore cavities can be modified. This unique feature is quite different from that of traditional porous zeolites whose pores are confined by a rigid

skeleton that is difficult to alter. This is why MOFs are quickly becoming very successful for research, aiming at industrial application in adsorption and catalytic technology[11–18].

Therefore, experimental and theoretical studies of the adsorptive properties of MOFs are of large importance to further extend their applicability. Inverse gas chromatography is one of the common techniques employed to determine the thermodynamic adsorption properties such as Henry adsorption constants, adsorption enthalpies and adsorption entropies at very low pressure and degree of pore filling, to better understand the interactions with the microporous in the material[19–22]. Using this technique, the shape selective behaviour of zeolites[19,23–29] and MOFs such as MIL-47[30], UiO-66[15,31], ZIFs[32,33], CuBTC[34], COMOC-2[35] and DUT-5[2] for linear/iso-alkane, linear/branched alkane isomers and for C8 alkylaromatic isomers has been studied.

In this work, low coverage adsorption properties of Al-Fumarate are studied. Al-Fumarate is a commercially available MOF that appeared for the first time in 2007[36]. It was proposed for storage and delivery of natural gas for automotive applications[37]. In spite of its commercial availability and environmentally friendly production process, it did not yet receive much attention in scientific literature. Only in 2013, Jeremias et al. measured water adsorption isotherms at temperatures comprised between 298 and 333 K and obtained maximum water loading of 0.45 g/g[38]. They brought out its stability towards water after 80 adsorption/desorption cycles. Recently Alvarez et al. modified the synthesis procedure of Al-Fumarate A520[39]. They obtained a more crystalline sample, denoted MIL-53 (Al)-FA, having less defect sites. Using this material, a structural model for the Al-Fumarate MOF, based on a combination of X-Ray Powder Diffraction, solid-state NMR, IR spectroscopy and a computational approach, was proposed. The structural determination lead to the same space group as the one obtained for the hydrated form of MIL-53 (Al). Indeed, Al-Fumarate, having the formula (Al (OH)-(O_2C-

C_2H_2-CO_2) $3.5H_2O$), and hydrated MIL-53 (Al), with the formula (Al(OH)(O_2C-C_6H_4-CO_2)$1H_2O$), are two isostructural MOFs; both are built from linear chains of AlO_4 $(OH)_2$ octahedra. The structure of those MOFs consists of infinite Al-OH-Al chains connected by organic linkers, generating 1-dimensional diamond shaped pores. In the case of MIL-53(Al), a terephthalate linker interconnects the AlO_4 $(OH)_2$ metal nodes, while in the case of Al-Fumarate, a fumarate linker is used to interconnect the metal nodes. Both form lozenge-shaped 1D pores but have different pore dimensions. The size of Al-Fumarate pores (5.7 x 6.0 A^2)[39] is smaller than that of MIL-53(Al)[40] because of the shorter length of the fumaric acid linker compared to terephtalic acid. While the structure of MIL-53(Al) clearly shows a pronounced breathing behaviour in contact with water or CO_2 [41,42], no such structural flexibility has been observed for Al-Fumarate. MIL-53(Al) is behaves in a non-shape selectivity manner in the adsorption of linear and branched alkanes; the adsorption properties are dominated by the Van der Waals interactions[43] while steric effects play no role. On the other hand, it has a pronounced preference for the ortho-isomers of C_8, C_9, and C_{10} alkylaromatics due to entropic effects which occur during the packing of such molecules in the MIL-53 (Al) pores[41] at high degree of pore filling.

In here, low coverage adsorption properties of linear, branched and cyclic alkanes and xylene isomers in Al-Fumarate are investigated using the inverse chromatographic technique. It is demonstrated that, as compared to MIL-53(Al), Al-Fumarate behaves in a much more selective way, imposing steric constraints on the adsorption of branched and cyclic alkanes resulting in pronounced shape selectivity.

1 Experimental

1.1 Material Synthesis

Al-Fumarate was synthesized according to a literature procedure[44]. To a round bottom flask 2.26 g of fumaric acid, 4.47 g of $AlCl_3 \cdot 6H_2O$ and 130 g of DMF were added and stirred under reflux for 17 hours. The formed powder was filtered off and washed with acetone. Subsequent washing cycles consisted of suspension in the washing solvent, sonication and filtration. Two cycles were conducted with acetone, followed by two cycles of methanol as solvent [44]. The Al-Fumarate structure was confirmed from X-ray powder diffraction data (Fig.S0).

1.2 Pulse gas chromatography

The pulse gas-chromatographic (GC) technique[45,46] was used to determine the adsorption properties of linear alkanes (*n*-pentane, *n*-hexane, *n*-heptane, *n*-octane), branched alkanes (2-methylbutane, 3-methylpentane, 3-methylhexane, 3-methylheptane, 2,3-dimethylbutane, 2,3-dimethylpentane, 2,5-dimethylhexane, 2,2,4-trimethylpentane), cycloalkanes (cyclohexane, cycloheptane, cyclo-octane), and aromatics (o-xylene, m-xylene, p-xylene) at high temperatures (150°C – 250°C) and at low surface coverage in the linear part of the adsorption isotherm. In order to avoid large pressure drops, aggregates of adsorbent crystals, called pellets, with thermal stability were prepared. The Al-Fumarate MOF powders were compacted into disks by applying a pressure of ca. 500 bar and the disks were broken into fragments and sieved. The 530–600 μ m fraction of the pelletized sample was used to fill an 1/8-inch diameter stainless steel column with a length of 30 cm. In situ activation of the adsorbents was

performed by raising temperature from room temperature to 250°C (1°C/min) and keeping the temperature stable for 6 hours. The gas flow was set to 10 NmL/min. Chromatograms were measured at temperatures between 150 and 250 °C using an AGILENT 4980D chromatograph with a thermal conductivity detector (TCD). The investigated components were injected (0.04 μ L) in an inert carrier gas (Helium) flowing at 19 NmL/min through the chromatographic column. The absence of external mass transport limitations was demonstrated by performing experiments at different carrier gas flow rates at 250°C with *n*-pentane (injected volume 0.04 uL), as shown in Fig.S2.

Henry adsorption constants were obtained from the first moment of the experimental chromatograms, as explained in earlier work[45–47]. From the temperature dependence of Henry's constant $K^{'}$, the enthalpy of adsorption ΔH_o and the pre-exponential factor $K^{'}{}_0$ of the van't Hoff equation can be determined:

$$K^{'} = K^{'}{}_0 \, exp\left(\frac{-\Delta H_o}{RT}\right) \quad (1)$$

The change in entropy during adsorption was calculated from the Gibbs energy of adsorption.

$$\Delta G_o = -RTln\left(K^{'} \rho_c RT\right) \quad (2)$$

Then, by reformulating the Gibbs energy equation, the entropy change can be calculated from the experimentally determined adsorption enthalpy and the computed ΔG_o :

$$\Delta S_o = \left[\frac{\Delta H_o - \Delta G_o}{T}\right] \quad (3)$$

An ideal separation factor between two components (A and B) at a given temperature was calculated as:

$$\alpha_0 = \frac{K_A^{'}(T)}{K'_B(T)}$$

To verify the stability and reusability of Al-Fumarate, some of the pulse-chromatographic experiments were repeated several months after the end of the experiments, using the column that was used for all the experiments and compared it to the original data. These experiments clearly demonstrate the reusability of the material in these experiments, as shown in Table S1.

1.3 Argon porosimetry

Pore volume and surface area were calculated from the argon adsorption isotherm measured at 87.45K. This measurement is realized by argon porosimetry (Argon source: Air Liquide, 99.999 %) using the Autosorb AS-1 (Quantachrome Instruments, United States) on a powder sample of Al-Fumarate, thermally activated at 250°C under vacuum (30 inch mercury vacuum). The reversible isotherm in Fig.S1 indicates a permanent porosity. A pore volume of 0.35 mL/g at a relative pressure of 0.21 is obtained via the Dubinin-Radushkevich (DR) method. A surface area of 879.5 m^2/g is obtained by calculation via the multipoint BET method using points in the relative pressure range between 0.05 and 0.35. Besides, an Argon isotherm was measured on the sample in pellet form, retrieved at the end of the experiments from the used column. Until a relative pressure of 0.01, the isotherms of the used sample (was kept for more than 6 months in the column) and the fresh sample (with Al-Fumarate structure as confirmed by XRD) completely coincide, demonstrating that the Al-Fumarate structure was fully retained. At higher pressure, a modest decrease of 7 % (at the relative pressure of 0.2) in pore volume was observed (Fig.S1), but this is rather due to a change in experimental parameters during the Ar isotherm measurement and the shaping procedure of powder into pellets (binderless).

2 Results and discussion

2.1 Argon porosimetry

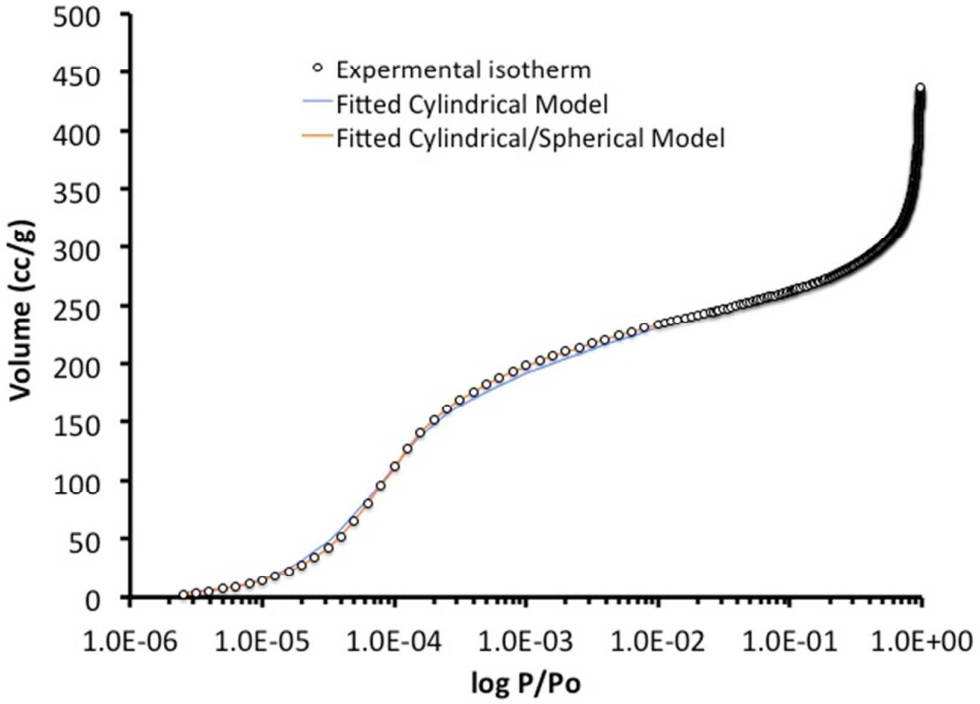

Fig. 1: Argon sorption isotherm of Al-Fumarate powder sample at 87.45 K

The Ar isotherm in Fig.1 and Fig.S1 (including the desorption isotherm) shows full reversibility and predominance of micropores. A pore size distribution was obtained with the DFT model by considering models developed for cylindrical/spherical and for cylindrical[48,49,50] pores The best fit is obtained with cylindrical/spherical model, giving a pore size distribution with a maximum at 4.15 Å of half pore width, which corresponds to a pore diameter of 8.30 Å. The cumulative pore volume stays constant at 0.43 cm^3/g above a pore diameter of 10 Å, indicating absence of mesopores. When considering the pore having a cylindrical form, the fit is slightly less good. This model gives a lower value of the pore size, with a pore diameter of 5.82 Å, as shown in Fig.2. The pore diameter

obtained by Alvarez et al from an N_2 isotherm using the methodology of Gelb and Gubbin is 5.8 Å for Al-Fumarate in its hydrated form[39].

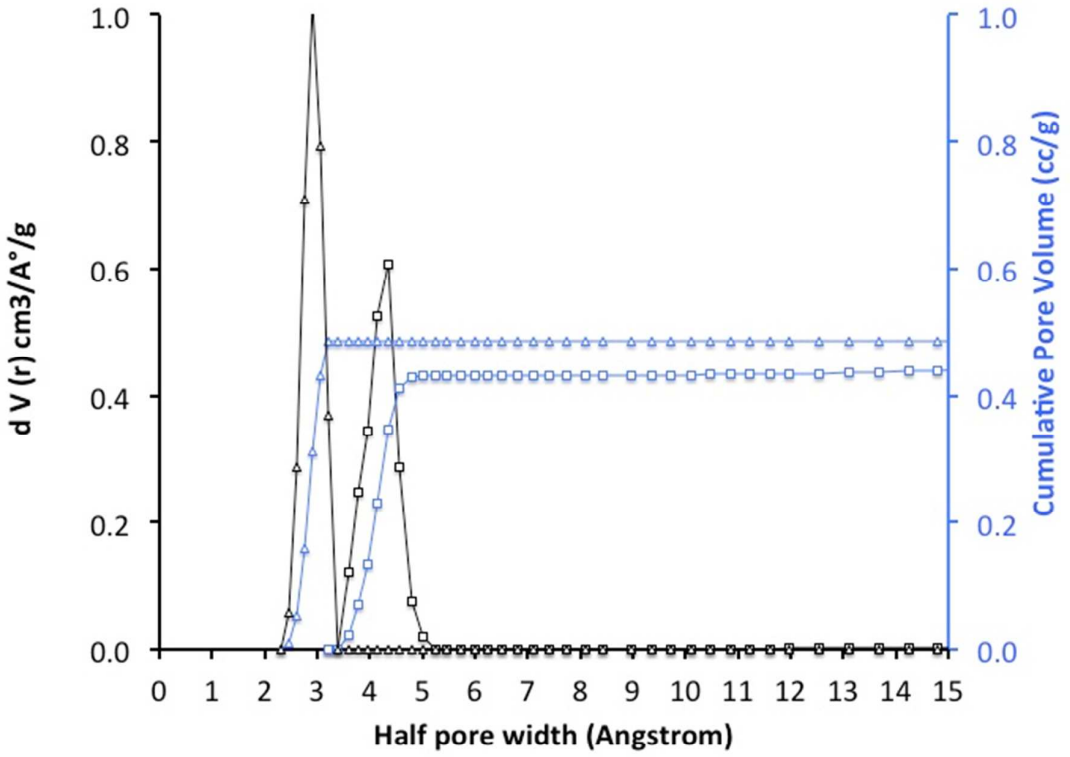

Fig. 2: Pore size distribution and cumulative volume curves obtained from the Ar isotherm at 87.45 K. Triangles represent the cylindrical model; squares represent the spherical/cylindrical model.

2.2 Pulse Chromatography

Chromatograms Low-coverage adsorption of linear, branched, cyclic alkanes (C_5-C_8) and aromatics was examined using the inverse chromatographic technique. As shown in Fig.3, Al-Fumarate shows large differences in retention for structural alkane isomers.

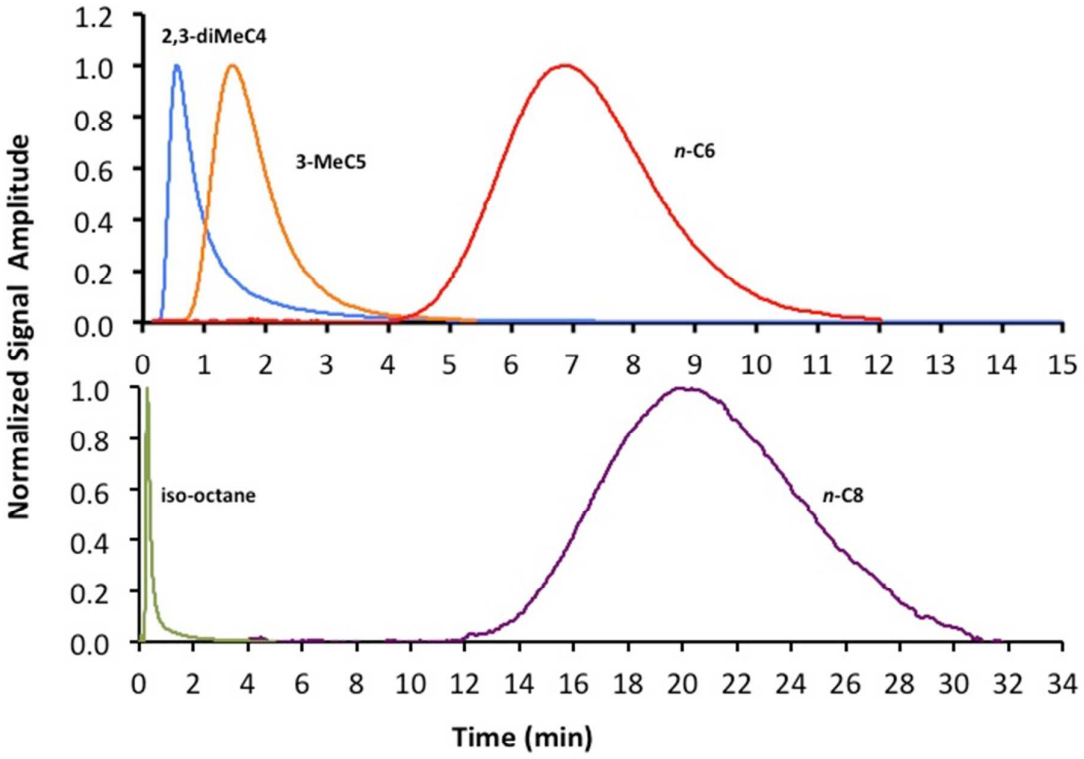

Fig. 3: Top: Chromatograms of *n*-C6, 3-MeC5 and 2,3-DiMeC4 at 210°C. Bottom: *n*-C8 and iso-C8 at 250°C.

Chromatograms of *n*-hexane (*n*-C6), 3-methylpentane (3-MeC5), 2,3-dimethylbutane (2,3-diMeC4) at 210 °C, and the chromatograms of *n*-octane (*n*-C8) and iso-octane (iso-C8) at 250°C on Al-Fumarate are shown in Fig.3. For molecules having 6 carbon atoms, *n*-C6 is retained the longest, with a first moment of the peak of 7.2 minutes. The first

molecule to elute is 2,3-diMeC4 followed by the monobranched isomer, 3-MeC5. *n*-C6 is retained about 4 times longer than 3-MeC5 and 8 times longer than 2,3-diMeC4. *n*-C8 is retained about 39 times longer than iso-C8 at 250°C, the latter compound almost eluting immediately from the column. Similar chromatograms are obtained for the heptane and octane isomers (not shown). It is thus clearly demonstrated that Al-Fumarate behaves in a selective manner, with linear alkanes being retained much stronger than their branched isomers. For comparison, on MIL-53(Al), the difference in retention time between *n*-C6 (26.9 minutes) and 2,3-dimethylbutane (24.8 min) is only a factor 1.08 at 160°C.

Moreover, cyclic molecules are also less retained than the linear structure (Fig.4) Cyclohexane (cC6) is retained 3 times less than its linear isomer *n*-C6 at 210 °C. Benzene elutes in between cC6 and *n*-C6. Also cycloheptane and cyclo-octane are retained much less than their linear isomers, with differences in retention of a factor 12.6 and 81.4.

As shown in Fig. 4, a clear separation is also achieved between xylene isomers, a series of molecules with similar boiling points that are difficult to separate using distillation or non-shape selective adsorbents[30]. Among the xylene isomers, the para form of xylene has the largest affinity followed by m-xylene and o-xylene. The retention time of p-xylene is about 3 times larger than that of o-xylene. This order of elution does not follow the order of boiling points (p-xylene: 138°C < m-xylene: 139°C < o-xylene: 144°C).

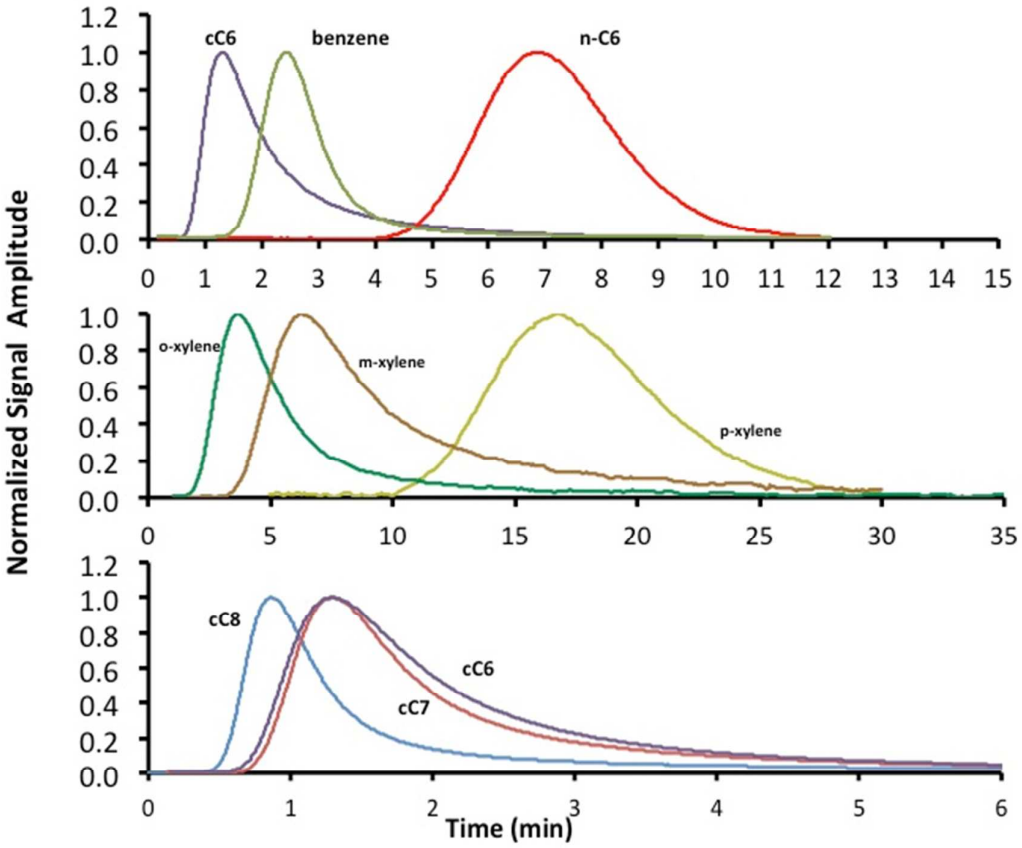

Fig. 4: Top: chromatograms of *n*-C6, benzene and cC6 at 210°C; Middle: and o, m, p–xylenes at 210°C; Bottom: cyclohexane, cycloheptane and cyclo-octane at 210°C

Henry constants – Adsorption enthalpies

As expected, the selectivity of the linear alkanes over their isomers decreases with temperature as illustrated in Fig.5. For monobranched and cyclic C6-alkanes, separation factors between 4 and 6 were observed. The selectivity increases with the degree of branching. Between *n*-C8 and iso-C8, the separation factor exceeds 100 at temperatures below 200°C, practically corresponding to the exclusion of this compound from adsorption.

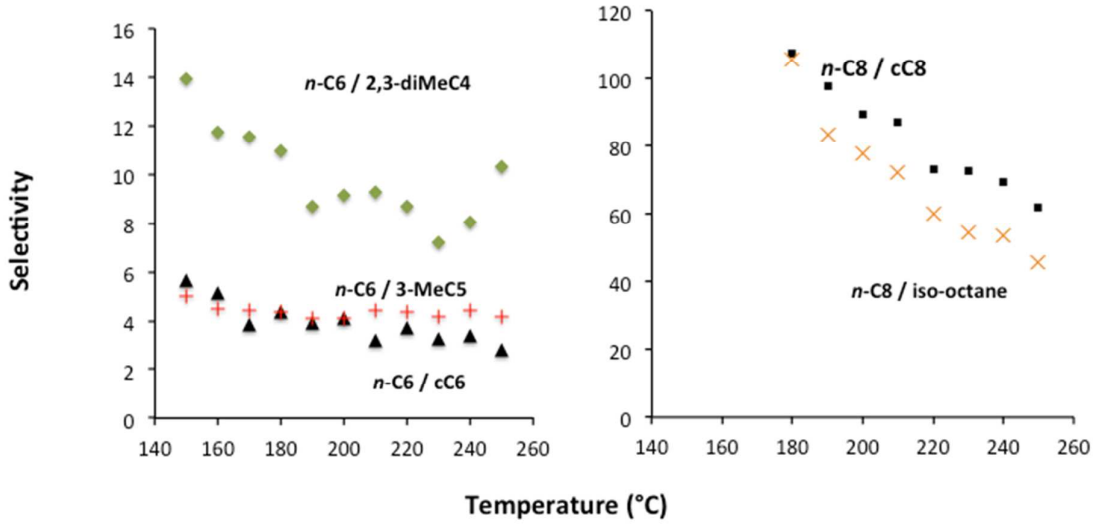

Fig. 5: Separation factors of alkanes versus their isomers as a function of temperature on Al-Fumarate

These large separation factors indicate that Al-Fumarate imposes steric constraints on the adsorption of branched and cyclo-alkanes. This selective property differentiates it from MIL-53(Al), a MOF with similar pore structure, since the latter material is non-shape selective for such molecules, with separation factors below 2[43]. To verify if the differences in adsorption between linear and branched alkanes on Al-Fumarate are caused by steric effects imposed by the structure of the adsorbent, rather than due to

the differences in physicochemical properties of the probe components, a plot of the logarithm of the vapor pressure versus the logarithm of the Henry constants is made (Fig.6). In the absence of shape selectivity, a unique relationship is observed for all components in such a plot[51]. Although linear correlations are obtained for both the linear and monobranched alkanes, the branched alkanes clearly follow a different relationship than the linear alkanes. For multibranched and cyclo-alkanes, the difference with the linear alkanes is even larger in this plot. This confirms that the large difference in Henry constants between these molecules is a consequence of steric constants and not the result of the different physicochemical properties of the molecules.

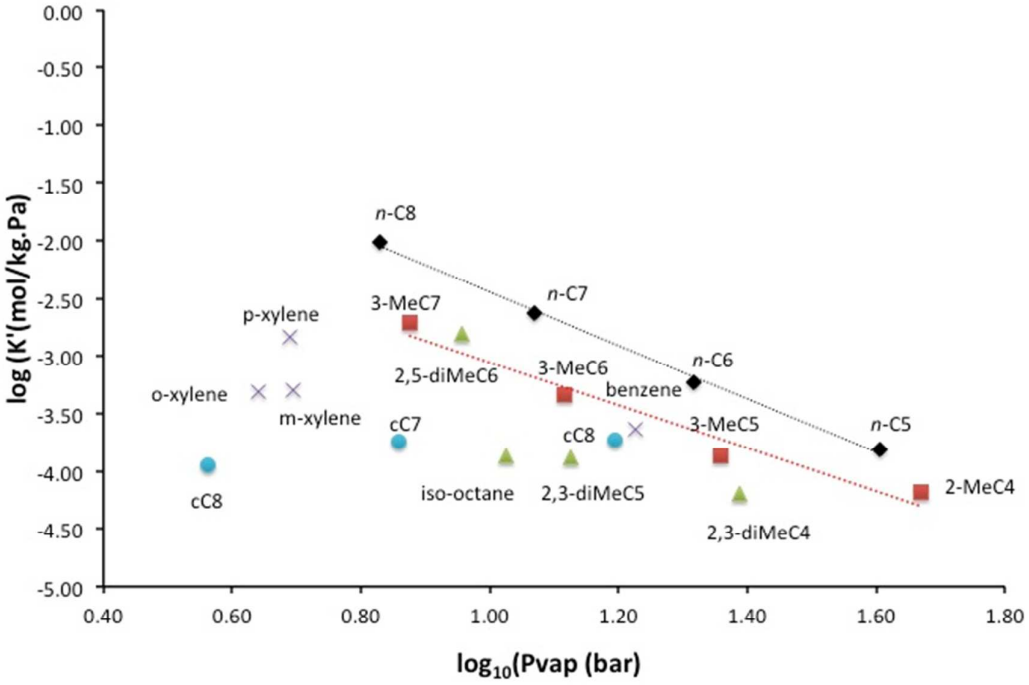

Fig. 6: Logarithm of Henry constants on Al-Fumarate at 210°C. Diamonds: linear alkanes; squares: mono-branched alkanes; triangles: di-branched alkanes; circles: cyclo-alkanes; crosses: arenes.

The temperature dependency of the Henry adsorption constant is in accordance with the van' t Hoff relation, with van 't Hoff plots having coefficients of determination, R^2,

between 0.992-0.999 (Fig.S3-S7). Henry adsorption constants, limiting adsorption enthalpies and entropies derived from the van 't Hoff plots, can be found in Table 1.

Table 1: Thermodynamic properties of different components on Al-Fumarate

Compound	K'@180°C (mol/kg/Pa)	ΔG_0@180°C (kJ/mol)	ΔS_0@180°C (J/mol/K)	ΔH_0 (kJ/mol)	$-\ln K'_0$ (mol/kg/Pa)
		Linear alkanes			
n-pentane	$(4.06 \pm 0.25)\ 10^{-4}$	-28.9 ± 7.3	-67.6 ± 3.5	-59.5 ± 1.1	23.6 ± 0.3
n-hexane	$(1.79 \pm 0.11)\ 10^{-3}$	-34.5 ± 7.2	-74.8 ± 3.5	-68.4 ± 1.1	24.5 ± 0.3
n-heptane	$(8.84 \pm 0.53)\ 10^{-3}$	-40.5 ± 7.3	-86.5 ± 4.0	-79.7 ± 1.1	25.9 ± 0.3
n-octane	$(4.19 \pm 0.25)\ 10^{-2}$	-46.4 ± 7.3	-90.8 ± 4.2	-87.5 ± 1.9	26.5 ± 0.5
		Branched alkanes			
2-methylbutane	$(1.79 \pm 0.11)\ 10^{-4}$	-25.8 ± 7.3	-72.7 ± 3.7	-58.8 ± 1.1	24.3 ± 0.3
3-methylpentane	$(4.09 \pm 0.25)\ 10^{-4}$	-28.9 ± 7.3	-82.4 ± 4.0	-66.3 ± 1.1	25.4 ± 0.3
3-methylhexane	$(1.67 \pm 0.10)\ 10^{-3}$	-34.2 ± 7.2	-92.2 ± 3.6	-76.1 ± 1.1	26.6 ± 0.3
3-methylheptane	$(8.37 \pm 0.50)\ 10^{-3}$	-40.3 ± 7.3	-100.7 ± 4.0	-86.0 ± 1.5	27.6 ± 0.4
2,3-dimethylbutane	$(1.64 \pm 0.10)\ 10^{-4}$	-25.5 ± 7.4	-68.7 ± 4.3	-56.8 ± 1.2	23.7 ± 0.4
2,3-dimethylpentane	$(4.74 \pm 0.29)\ 10^{-4}$	-29.5 ± 7.3	-86.8 ± 3.6	-68.5 ± 1.1	26.0 ± 0.4
2,5-dimethylhexane	$(6.94 \pm 0.42)\ 10^{-3}$	-39.6 ± 7.3	-95.7 ± 4.4	-82.6 ± 1.1	27.0 ± 0.3
iso-octane	$(3.96 \pm 0.24)\ 10^{-4}$	-28.8 ± 7.3	-79.5 ± 3.6	-64.8 ± 1.1	25.1 ± 0.3
		Cyclo-alkanes			
cyclohexane	$(4.13 \pm 0.25)\ 10^{-4}$	-29.0 ± 7.3	-63.9 ± 3.5	-57.9 ± 1.0	23.1 ± 0.3
cycloheptane	$(4.76 \pm 0.29)\ 10^{-4}$	-29.5 ± 8.9	-67.3 ± 3.7	-60.0 ± 1.1	23.5 ± 0.3
cyclo-octane	$(3.90 \pm 0.24)\ 10^{-4}$	-28.8 ± 7.3	-96.1 ± 3.8	-72.3 ± 1.1	27.1 ± 0.3
		Arenes			
benzene	$(5.84 \pm 0.35)\ 10^{-4}$	-30.3 ± 7.2	-30.3 ± 3.4	-57.4 ± 1.6	22.7 ± 0.5
o-xylene	$(1.57 \pm 0.09)\ 10^{-3}$	-34.0 ± 7.2	-89.5 ± 3.7	-74.6 ± 1.1	26.3 ± 0.3
m-xylene	$(1.68 \pm 0.10)\ 10^{-3}$	-34.3 ± 7.2	-89.6 ± 3.6	-74.9 ± 1.1	26.2 ± 0.3
p-xylene	$(5.65 \pm 0.34)\ 10^{-3}$	-38.8 ± 7.2	-3.7 ± 3.6	-76.8 ± 1.1	25.6 ± 0.3

For the *n*-alkanes and monobranched alkanes, Henry adsorption constants increase in an exponential way with carbon number N_C (Fig.S9). Remarkably, this is not the case for the cyclo-alkanes, which all have comparable Henry constants (see Table 1). The Henry adsorption constants of the branched alkanes, cyclo-alkanes and arenes are in each case significantly lower than those of the linear alkane with corresponding carbon number on this microporous MOF.

For the *n*- and monobranched alkanes, a linear correlation between the adsorption enthalpy and N_c is observed (Fig.S8). For each additional $-CH_2-$ group, the zero coverage adsorption enthalpy increases with 9.7 and 9.1 kJ/mol respectively for linear and mono-branched alkanes. Moreover, the difference in adsorption enthalpy between multi-branched or cyclo-alkanes and their linear isomers in Al-Fumarate is large. For example, the difference in adsorption enthalpy amounts 22.7 kJ/mol and 11.6 kJ/mol between iso-C8 and *n*-C8, and 2,3-dimethylbutane/*n*-C6 respectively. Such significant differences in interaction between linear and branched alkanes are not observed with similar types of frameworks such as MIL-47 and MIL-53(Al), where the adsorption enthalpy of *n*- and iso-alkanes only differs by a few kJ/mol, as put in evidence by Finsy et al[43].

No large difference in adsorption enthalpy is observed between benzene and cC6, whereas their enthalpies are considerably lower than that of *n*-C6 (Table 1). The same conclusion holds for cyclo-octane, *n*-octane and the xylene isomers. The adsorption enthalpy of o-xylene, m-xylene and p-xylene are similar. Specific interactions between the Al-Fumarate framework and the π-electrons of the arenes are thus low to negligible, in spite of the presence of a double bond in the organic linker of the framework. The interaction potential is dominated by non-specific Van der Waals forces.

The zero coverage adsorption entropy gives supplementary information about the loss of freedom ($\Delta \boldsymbol{S_o} < 0$) during the process of adsorption. The adsorption entropy is directly reflected by the pre-exponential factor $\boldsymbol{K_0}$. Direct interpretation of the adsorption entropy is not facile; a so-called compensation chart gives the more straightforward possibility to compare the variation of freedom ($\Delta \boldsymbol{S_o}$) of the molecules for a fixed interaction ($\Delta \boldsymbol{H_0}$) for various types of molecules.

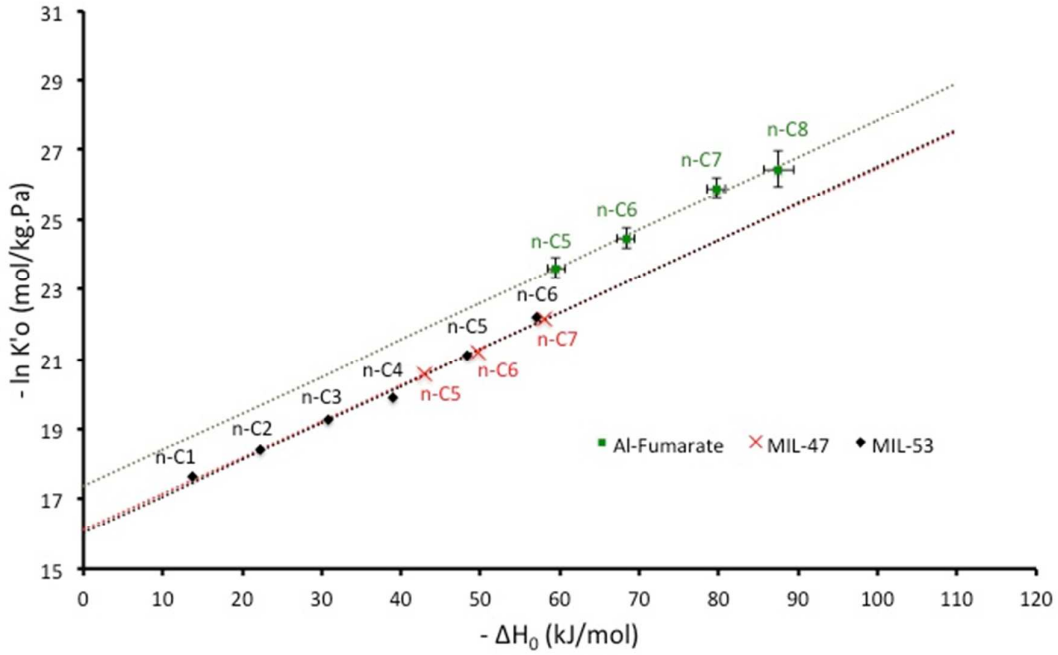

Fig.7: Compensation chart of linear alkanes on Al-Fumarate, MIL-53 and MIL-47

For comparison, data for *n*-alkanes on MIL-47 and MIL-53(Al) were added in Fig.7. As often observed, $\ln K'_0$ varies in linear way with - ΔH_o for the *n*-alkanes[52]. The longer the chain, the stronger the interaction between the molecule and the surface atoms in the pores and in turn, the larger the loss of freedom. The compensation chart shows an identical linear relationship between pre-exponential factors and adsorption enthalpy for MIL-47 and MIL-53. Both materials have an identical pore size and structure; therefore molecules loose the same amount of freedom. Interestingly, Al-Fumarate

shows a different correlation between adsorption entropy and enthalpy. First of all, it is observed that all *n*-alkanes have significantly larger adsorption enthalpies on Al-Fumarate as compared to MIL-47 and MIL-53(Al). For example, $-\Delta H_0$ of *n*-C5 equals 60 kJ/mol on Al-fumarate, 48 kJ/mol on MIL-53(Al) and 43 kJ/mol on MIL-47.

Secondly, for a given adsorption enthalpy (energetic interaction), more negative values for $\ln K'_0$ are obtained, which corresponds to a lower number of adsorption sites and/or a larger loss of freedom on Al-Fumarate. Thirdly, the slope of the compensation chart is similar on the 3 materials. It has been suggested before that the slope of this curve reflects the actual pore size or degree of confinement in the adsorbent, as discussed in more detail further on.

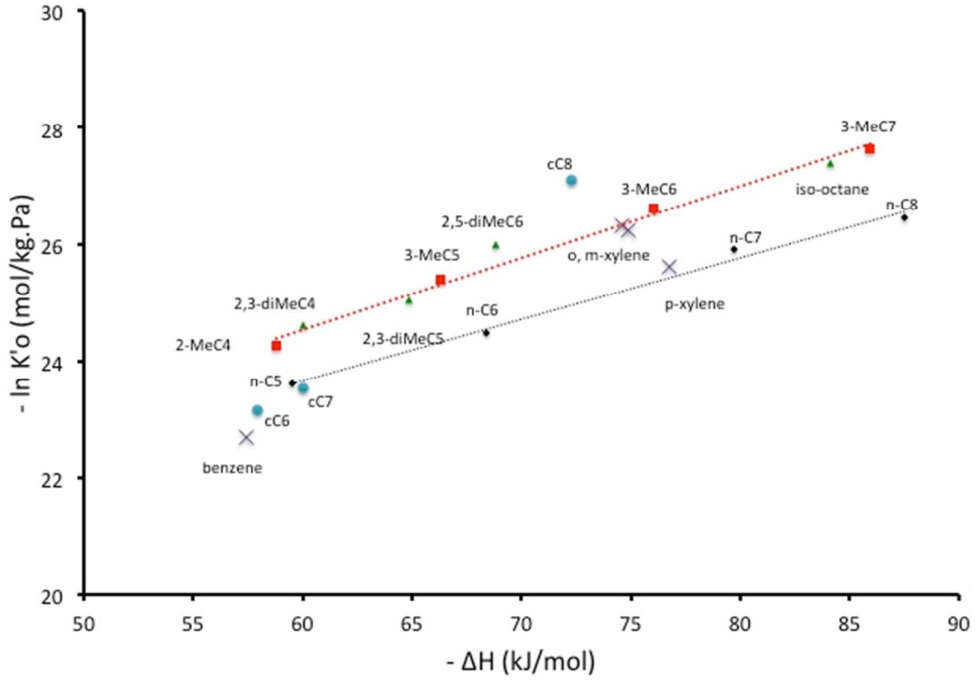

Fig.8: Compensation chart of linear and branched alkanes on Al-Fumarate. Diamonds: linear alkanes; squares: mono-branched alkanes; triangles: di-branched alkanes; circles: cyclo-alkanes; crosses: arenes.

Remarkably, a linear relation is also observed in the compensation chart in Fig.8 for iso-alkanes, including monobranched, dibranched and even tribranched alkanes. The compensation line for these branched alkanes is shifted upwards and has a larger slope, which corresponds to a larger loss of freedom. Only few molecules (benzene, p-xylene, cyclohexane and cyclo-octane) deviate from this tendency, pointing at a subtle interplay between molecular shape and the pore structure.

3 Discussion

In comparison to materials with a similar pore topology (MIL-53(Al) and MIL-47), Al-Fumarate behaves in a much more discriminative manner with respect to the adsorption of molecules of different shape. It clearly shows shape selectivity in the adsorption of branched and cyclo-alkanes and allows their chromatographic separation (Fig 4-5), with separation factors by far exceeding those of MIL-53(Al) and MIL-47 (Fig. 6). Al-Fumarate also allows separation of para-, ortho- and meta-xylene, structural isomers with respective critical diameters of 5.8 Å, 6.8 Å and 6.8 Å, at low pressure. In order to achieve this separation, a close match between the molecules and the pores is required.

The obtained separation factors are in fact comparable to those obtained on shape selective zeolites with pore sizes between 5 and 7 Å, such as ZSM-5, Beta and Mordenite[8]. This is in line with the earlier reported pore size of 5.7 x 6.0 A^2 for Al-Fumarate pores[35], and also with the pore diameter of 5.82 Å obtained by applying a cylindrical pore model to the Argon isotherm measured in this work (vide supra). The pore diameter of 8.30 Å obtained using a cylindrical/spherical model seems an overestimation of the actual pore size, as pores of this size are not expected to behave in such a shape selective manner. The critical diameter of the alkanes increases in the following order: *n*-alkanes (4.3 Å) < mono-branched alkanes (~5.0 Å) < multibranched

alkanes with vicinal methyl side chains (~5.8 Å) < multibranched alkanes with quaternary carbon atom (~6.3 Å). The very large separation factor between *n*-octane and 2,2,4-trimethylpentane suggests a pore size close to 6 Å.

For all tested hydrocarbons, the adsorption enthalpy (Table 1) and its evolution with N_c is superior to that of MIL-53(Al) and MIL-47, which have a pore size of about 8.5 x 8.5 A^2 (MIL-53) and 10.5 x 11.0 A^2(MIL-47). For linear alkanes, the heat of adsorption increases with respectively 9.7 kJ/mol on Al-Fumarate, 8.7 kJ/mol on MIL-53(Al) and 7.5 kJ/mol on MIL-47 per additional $–CH_2-$ group. It is well known that Van der Waals interactions become larger with decreasing pore size. The more negative values for the pre-exponential factors in the compensation chart (Fig.7) also point at larger losses of freedom as compared to MIL-53(Al) and MIL-47. On the other hand, it is surprising that the slope of the compensation chart is nearly identical for these 3 materials; in our earlier work with zeolites[53,54], we found that smaller pore sizes lead to a larger slope (confinement factor) of the compensation chart. More work is needed to understand this phenomenon.

4 Conclusions

In this work, it is shown that Al-Fumarate allows separation linear, branched and cyclic alkanes. Moreover, it also separates xylene isomers from each other. It was found that the adsorptive interactions are dominated by aspecific Van der Waals interactions. By determining the correlation between the Henry constants of linear, branched, cyclic and aromatic alkanes and their vapour pressure, we put in evidence the shape selective behaviour of the Al-Fumarate Metal-Organic Framework in low coverage conditions. The graphic representation of this correlation clearly discriminates the separation based

on physicochemical effects of the injected alkane probes. Moreover, the large separation factors between linear and branched or cyclic alkanes indicate that the separation of Al-Fumarate is based on the sterical effects. In comparison to its isostructural MOFs, MIL-53(Al) and MIL-47, its behaviour is clearly different and much more selective. This distinction is due to its significantly lower pore size. An analysis of the adsorption data reveals an effective pore size close to 6 Å, in agreement with structural analysis and porosimetry data of other studies[39].

Acknowledgements

The authors are grateful to IWT Vlaanderen, for financial support for the MOFShape project.

1 D. M.Ruthven, *Principle of adsorption and adsorption processes*, 1984.

2 S. Couck, Y.-Y. Liu, K. Leus, G. V. Baron, P. Van der Voort and J. F. M. Denayer, *Microporous Mesoporous Mater.*, 2015, **206**, 217–225.

3 P. B. Weisz and V. J. Frilette, *J. Phys. Chem.*, 1960, **64**, 382–382.

4 R. Madon, *J. Catal.*, 1991, **129**, 275–287.

5 K. Huddersman and M. Klimczyk, *J. Chem. Soc. Faraday Trans.*, 1996, **92**, 143.

6 K. Huddersman and M. Klimczyk, *AIChE J.*, 1996, **42**, 405–408.

7 C. L. Cavalcante and D. M. Ruthven, 1994, 1209–1216.

8 J. F. Denayer, W. Souverijns, P. a. Jacobs, J.A. Martens and G. V. Baron, *J. Phys. Chem. B*, 1998, **102**, 4588–4597.

9 J. F. M. Denayer, R. a. Ocakoglu, J. Thybaut, G. Marin, P. Jacobs, J. Martens and G. V. Baron, *J. Phys. Chem. B*, 2006, **110**, 8551–8558.

10 H. K. Chae, D. Y. Siberio-Pérez, J. Kim, Y. Go, M. Eddaoudi, A. J. Matzger, M. O'Keeffe and O. M. Yaghi, *Nature*, 2004, **427**, 523–527.

11 B. Chen, C. Liang, J. Yang, D. S. Contreras, Y. L. Clancy, E. B. Lobkovsky, O. M. Yaghi and S. Dai, *Angew. Chemie Int. Ed.*, 2006, **45**, 1390–1393.

12 C. Serre, S. Bourrelly, A. Vimont, N. a. Ramsahye, G. Maurin, P. L. Llewellyn, M. Daturi, Y. Filinchuk, O. Leynaud, P. Barnes and G. Férey, *Adv. Mater.*, 2007, **19**, 2246–2251.

13 F. Vermoortele, R. Ameloot, A. Vimont, C. Serre and D. De Vos, *Chem. Commun.*

(Camb)., 2011, **47**, 1521–3.

14 E. Keceli, M. Hemgesberg, R. Grünker, V. Bon, C. Wilhelm, T. Philippi, R. Schoch, Y. Sun, M. Bauer, S. Ernst, S. Kaskel and W. R. Thiel, *Microporous Mesoporous Mater.*, 2014, **194**, 115–125.

15 P. S. Bárcia, D. Guimarães, P. a. P. Mendes, J. a. C. Silva, V. Guillerm, H. Chevreau, C. Serre and A. E. Rodrigues, *Microporous Mesoporous Mater.*, 2011, **139**, 67–73.

16 P. a. P. Mendes, P. Horcajada, S. Rives, H. Ren, A. E. Rodrigues, T. Devic, E. Magnier, P. Trens, H. Jobic, J. Ollivier, G. Maurin, C. Serre and J. a. C. Silva, *Adv. Funct. Mater.*, 2014, **24**, 7666–7673.

17 H.-C. Zhou, J. R. Long and O. M. Yaghi, *Chem. Rev.*, 2012, **112**, 673–674.

18 N. Stock and S. Biswas, *Chem. Rev.*, 2012, **112**, 933–969.

19 X. Zhang, L. Qian, P. Xu, H. He and Q. Du, *Chem. Eng. J.*, 2008, **137**, 579–586.

20 F. Miano, *Colloids Surfaces A Physicochem. Eng. Asp.*, 1996, **110**, 95–104.

21 X. Canet, J. Nokerman and M. Frère, *Adsorption*, 2005, **11**, 213–216.

22 E. Díaz, S. Ordóñez, A. Vega and J. Coca, *J. Chromatogr. A*, 2004, **1049**, 161–169.

23 A. Kondor and A. Dallos, *J. Chromatogr. A*, 2014, **1362**, 250–261.

24 H. Jin, E. A. Prasetyanto, N. Jiang, S.-M. Oh and S.-E. Park, *Appl. Surf. Sci.*, 2010, **256**, 5508–5512.

25 J. Nokerman, X. Canet, P. Mougin, S. Limborg-Noetinger and M. Frère, *Meas. Sci. Technol.*, 2005, **16**, 1802–1812.

26 E. Díaz, S. Ordóñez and A. Auroux, *J. Chromatogr. A*, 2005, **1095**, 131–137.

27 I. C. Arik, J. F. Denayer and G. V. Baron, *Microporous Mesoporous Mater.*, 2003, **60**, 111–124.

28 F. Tümsek and O. İnel, *Chem. Eng. J.*, 2003, **94**, 57–66.

29 A. Aşkin and O. İnel, *Sep. Sci. Technol.*, 2001, **36**, 381–397.

30 L. Alaerts, C. E. A. Kirschhock, M. Maes, M. A. van der Veen, V. Finsy, A. Depla, J. A. Martens, G. V. Baron, P. A. Jacobs, J. F. M. Denayer and D. E. De Vos, *Angew. Chemie*, 2007, **119**, 4371–4375.

31 B. Bozbiyik, T. Duerinck, J. Lannoeye, D. E. De Vos, G. V. Baron and J. F. M. Denayer, *Microporous Mesoporous Mater.*, 2014, **183**, 143–149.

32 S. Van Der Perre, T. Van Assche, B. Bozbiyik, J. Lannoeye, D. E. De Vos, G. V. Baron and J. F. M. Denayer, *Langmuir*, 2014, **30**, 8416–8424.

33 R. Krishna, *Phys. Chem. Chem. Phys.*, 2015, **17**, 39–59.

34 V. Finsy, L. Alaerts, D. De Vos, G. V Baron and J. F. M. Denayer, *From Zeolites to Porous Mof Mater. 40th Anniv. Int. Zeolite Conf. Proc. 15th Int. Zeolite Conf.*, 2007, **3**, 3–4.

35 S. Couck, T. R. C. Van Assche, Y.-Y. Liu, G. V. Baron, P. Van Der Voort and J. F. M. Denayer, *Langmuir*, 2015, **31**, 5063–5070.

36 *Ger. Pat.*, 2007.

37 M. Gaab, N. Trukhan, S. Maurer, R. Gummaraju and U. Müller, *Microporous Mesoporous Mater.*, 2012, **157**, 131–136.

38 F. Jeremias, D. Fröhlich, C. Janiak and S. K. Henninger, *RSC Adv.*, 2014, **4**, 24073.

39 E. Alvarez, N. Guillou, C. Martineau, B. Bueken, B. Van De Voorde, C. Le Guillouzer, P. Fabry, F. Nouar, F. Taulelle, D. De Vos, J. Chang, K. H. Cho, N. Ramsahye, T. Devic, M. Daturi, G. Maurin and C. Serre, *Angew. Chem. Int. Ed.*, 2015, **54**, 3664–3668.

40 T. Loiseau, C. Serre, C. Huguenard, G. Fink, F. Taulelle, M. Henry, T. Bataille and G. Férey, *Chem. - A Eur. J.*, 2004, **10**, 1373–1382.

41 C. Serre, F. Millange, C. Thouvenot, M. Noguès, G. Marsolier, D. Louër and G. Férey, *J. Am. Chem. Soc.*, 2002, **124**, 13519–13526.

42 P. L. Llewellyn, S. Bourrelly, C. Serre, Y. Filinchuk and G. Férey, *Angew. Chemie - Int. Ed.*, 2006, **45**, 7751–7754.

43 V. Finsy, VUB, 2009.

44 C. Kiener, U. Muller and M. Schubert, *US Pat. App. 12/297,666*, 2009, 1, 1–9.

45 J. F. Denayer, a. R. Ocakoglu, W. Huybrechts, J. a. Martens, J. W. Thybaut, G. B. Marin and G. V. Baron, *Chem. Commun.*, 2003, 15, 1880.

46 F. Tielens, J. F. M. Denayer, I. Daems, G. V. Baron, W. J. Mortier and P. Geerlings, *J. Phys. Chem. B*, 2003, **107**, 11065–11071.

47 J. F. M. Denayer, R. a. Ocakoglu, I. C. Arik, C. E. a. Kirschhock, J. a. Martens and G. V. Baron, *Angew. Chemie*, 2005, **117**, 404–407.

48 J. Landers, G. Y. Gor and A. V. Neimark, *Colloids Surfaces A Physicochem. Eng. Asp.*, 2013, **437**, 3–32.

49 M. Thommes, *Chemie Ing. Tech.*, 2010, **82**, 1059–1073.

50 M. Thommes and K. Cychosz, *Adsorption*, 2014, **20**, 233–250.

51 L. I. Devriese, J. a. Martens, J. W. Thybaut, G. B. Marin, G. V. Baron and J. F. M. Denayer, *Microporous Mesoporous Mater.*, 2008, **116**, 607–613.

52 T. Duerinck, S. Couck, F. Vermoortele, D. E. De Vos, G. V. Baron and J. F. M. Denayer, *Langmuir*, 2012, **28**, 13883–13891.

53 J. F. Denayer, A. Bouyermaouen and G. V. Baron, *Ind. Eng. Chem. Res.*, 1998, **37**, 3691–3698.

54 I. Daems, P. Leflaive, A. Méthivier, G. V. Baron and J. F. M. Denayer, *Microporous Mesoporous Mater.*, 2006, **96**, 149–156.